npj Computational Materials

www.nature.com/npjcompumats

ARTICLE OPEN

Check for updates

Giant room temperature elastocaloric effect in metal-free thin-film perovskites

Cheng Li[1,5], Yu Hui Huang[1,5]✉, Jian-Jun Wang[2,5]✉, Bo Wang[2], Yong Jun Wu[1,3], He Tian[4], Long-Qing Chen[2] and Zijian Hong[1,3]✉

Solid-state refrigeration which is environmentally benign has attracted considerable attention. Mechanocaloric (mC) materials, in which the phase transitions can be induced by mechanical stresses, represent one of the most promising types of solid-state caloric materials. Herein, we have developed a thermodynamic phenomenological model and predicted extraordinarily large elastocaloric (eC) strengths for the (111)-oriented metal-free perovskite ferroelectric $[MDABCO](NH_4)I_3$ thin-films. The predicted room temperature isothermal eC $\Delta S_{eC}/\Delta\sigma$ (eC entropy change under unit stress change) and adiabatic eC $\Delta T_{eC}/\Delta\sigma$ (eC temperature change under unit stress change) for $[MDABCO](NH_4)I_3$ are $-60.0\ J\ K^{-1}\ kg^{-1}\ GPa^{-1}$ and $17.9\ K\ GPa^{-1}$, respectively, which are 20 times higher than the traditional ferroelectric oxides such as $BaTiO_3$ thin films. We have also demonstrated that the eC performance can be improved by reducing the Young's modulus or enhancing the thermal expansion coefficient (which could be realized through chemical doping, etc.). We expect these discoveries to spur further interest in the potential applications of metal-free organic ferroelectrics materials towards next-generation eC refrigeration devices.

npj Computational Materials (2021)7:132 ; https://doi.org/10.1038/s41524-021-00599-1

INTRODUCTION

Solid-state refrigeration has attracted considerable attention due to its potential applications in small-scale cooling technology[1–3]. There are several physical effects that can be utilized for solid-state refrigeration, such as magnetocaloric (MC)[4,5], electrocaloric (EC)[6–9], and mechanocaloric (mC) effects[10,11]. In MC and EC effects, a temperature change is induced by applying a magnetic field and electric field, respectively. However, the MC and EC strengths for typical ferromagnetic/ferroelectric materials are relatively small. For instance, the EC strengths for prototype ferroelectrics such as $PbZr_{0.95}Ti_{0.05}O_3$[12] and fluorinated polymers[13] thin films are less than $1.0\ K\ m\ MV^{-1}$. To achieve a large temperature change, a strong magnetic/electric field is required, which is normally provided by a huge auxiliary device, limiting the practical applications of the MC/EC materials in cooling devices[9,14,15].

The mC effect[10], the application of a mechanical force that induces thermal cooling, can be divided into two categories, elastocaloric (eC) and barocaloric (BC) effects, for which the driving mechanical forces are uniaxial stress and hydrostatic pressure, respectively. The schematic illustration of an eC refrigeration cycle for thin films is shown in Fig. 1. The refrigeration cycle begins with applying a compressive stress on the film adiabatically (**step a**), the temperature rises from T_0 to T_{max} due to the release of latent heat. Then followed by the heat transfer from thin films to the surroundings (**step b**), with a decrease of temperature while the compressive stress is kept constant. The temperature keeps dropping when the compressive stress is gradually reduced (**step c**), as a result of the inverse eC effect. Finally, at **step d**, the compressive stress is fully removed. The film absorbs heat from the surroundings where the temperature rises back to T_0 after a full refrigeration cycle.

To maximize the temperature change and improve the energy efficiency for the cooling cycle, materials with high eC strength are required. Previously, high eC strength with $\Delta T_{eC}/\Delta\sigma$ of $0.7\ K\ GPa^{-1}$ has been predicted for ferroelectric oxide heterostructures such as $BaTiO_3$ thin films[1]. One key factor limiting the eC performance of the oxide ferroelectrics is their low compressibility with strong ionic bonds. Even though a high adiabatic temperature change might be obtained by applying large external stress, the eC strength is quite small which gives rise to low energy efficiency for a refrigeration cycle.

Recently, Wang et al. predicted extraordinarily large EC strengths, $18\ J\ m\ kg^{-1}\ K^{-1}\ MV^{-1}$ for the isothermal $\Delta S_{EC}/\Delta E$ and $8.06\ K\ m\ V^{-1}$ for the adiabatic $\Delta T_{EC}/\Delta E$, of a metal-free perovskite ferroelectric material $[MDABCO](NH_4)I_3$ (MDABCO stands for *N*-methyl-*N*′-diazabicyclo[2.2.2]octonium)[16], which is superior to the prototype perovskites[1,17–21] such as $BaTiO_3$ and $PbTiO_3$. For instance, the EC strength of $[MDABCO](NH_4)I_3$ is three times higher than the largest reported values of $BaTiO_3$, which could be attributed to the larger Curie–Weiss constant and smaller mass density of $[MDABCO](NH_4)I_3$. In addition to the smaller mass density, the molecular ferroelectric material has a much smaller elastic stiffness (~1 GPa) in comparison to typical ferroelectric oxides (~100 GPa). Therefore, it is rational to believe that large volume and entropy changes could be induced by applying external mechanical stimuli to $[MDABCO](NH_4)I_3$, which may generate a significant mC effect.

The very large BC effect was also reported in plastic crystals which are featured by the extensive disorder and giant compressibility[22,23]. For example, The BC strength $\Delta S/\Delta\sigma$ for NPG plastic crystals can reach $961.5\ J\ K^{-1}\ kg^{-1}\ GPa^{-1}$ at 320 K[22]. The metal-free organic perovskite ferroelectric $[MDABCO](NH_4)I_3$ is

[1]Laboratory of Dielectric Materials, School of Materials Science and Engineering, Zhejiang University, Hangzhou, China. [2]Department of Materials Science and Engineering, The Pennsylvania State University, University Park, PA, USA. [3]Cyrus Tang Center for Sensor Materials and Applications, State Key Laboratory of Silicon Materials, School of Materials Science and Engineering, Zhejiang University, Hangzhou, China. [4]Center of Electron Microscopy, State Key Laboratory of Silicon Materials, School of Materials Science and Engineering, Zhejiang University, Hangzhou, China. [5]These authors contributed equally: Cheng Li, Yu Hui Huang, Jian-Jun Wang. ✉email: huangyuhui@zju.edu.cn; jzw12@psu.edu; hongzijian100@zju.edu.cn

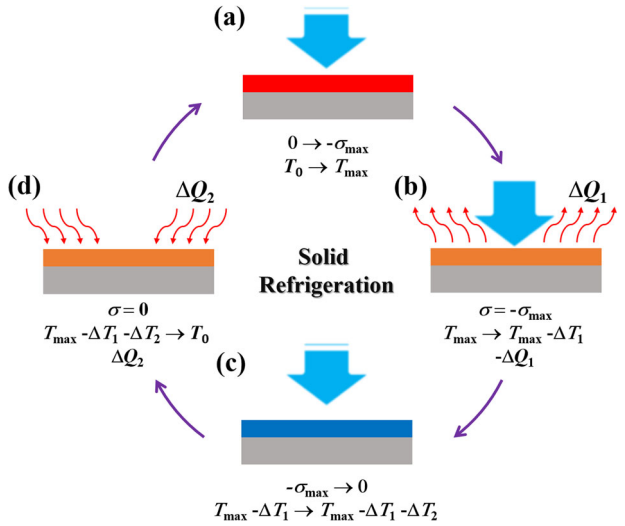

Fig. 1 Schematics of an eC refrigeration cycle. The cycle is divided into four steps: (**a**) compressive stress applying on the elastocaloric material, the release of latent heat and related temperature rise, (**b**) heat transfer to the surroundings when the stress is fixed at σ_{max}, (**c**) compressive stress removed gradually, uptake of latent heat and related temperature drop, (**d**) heat transfer to the elastocaloric material when the stress is fixed at 0. Elevated temperatures are represented in red and orange, decreased temperatures are in blue.

held together by both ionic and hydrogen-bonding interactions, which has considerably large compressibility. Large piezoelectric response was also predicted in [MDABCO]$(NH_4)I_3$ from first-principles calculations[24]. Moreover, [MDABCO]$(NH_4)I_3$ also has advantages of high polarization, mechanical flexibility, low weight, and low processing temperatures[25–31], as compared to other organic ferroelectric systems.

Computational methods such as thermodynamic calculations have emerged as powerful tools to the understanding of eC effects,[1,32–36] which could help to explain and design materials with high eC effects. In this work, we employ thermodynamic calculations to study the polarization properties and phase transitions of (111)-oriented ferroelectric [MDABCO]$(NH_4)I_3$ thin films under different combinations of in-plane misfit strains and out-of-plane stresses, from which the eC properties are calculated. As compared to the bulk system, thin films are much smaller in size which is beneficial to the miniature of the device, while also providing an extra degree of freedom (the substrate strain) in the design of the cooling device. It is revealed that the isothermal $\Delta S_{eC}/\Delta\sigma$ and adiabatic $\Delta T_{eC}/\Delta\sigma$ for a [MDABCO]$(NH_4)I_3$ thin film under an out-of-plane compressive stress of 1.28 GPa and in-plane isotropic misfit strain of 0.01 at 300 K can reach as high as −60.0 J K^{-1} kg^{-1} GPa^{-1} and 17.9 K GPa^{-1}, respectively, much superior to the traditional ferroelectric oxides. The giant eC effect is found to be attributed to the low Young's modulus and high thermal expansion coefficient of [MDABCO]$(NH_4)I_3$.

RESULTS

Phase transitions and phase diagram

The detailed procedure for developing a thermodynamic potential energy density function for (111)-oriented [MDABCO]$(NH_4)I_3$ film is described in the Theoretical Method Section and Supporting Information. The parameters for this study are all taken from the previous report[16]. We first calculate the analytical equilibrium polarization for the (111)-oriented [MDABCO]$(NH_4)I_3$ thin film under different in-plane misfit strains and out-of-plane stresses at room temperature. Consider a single-domain (111)-oriented thin film epitaxially grown on a cubic substrate with in-plane

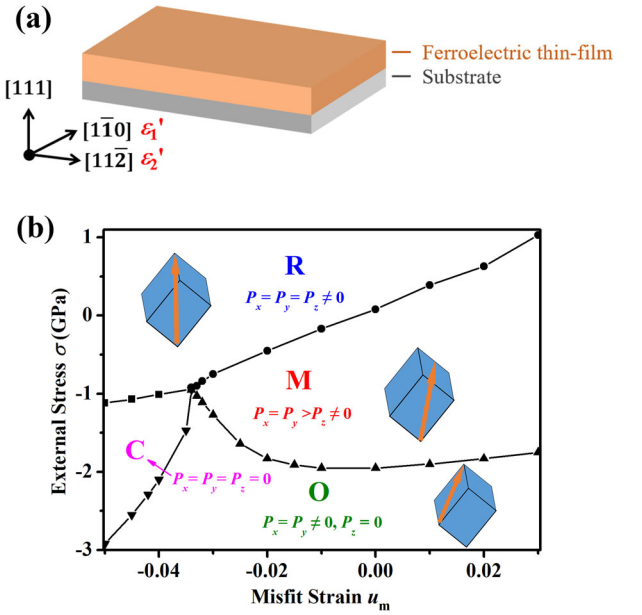

Fig. 2 Thin film model and misfit strain-stress phase diagram for (111)-oriented [MDABCO]$(NH_4)I_3$ thin film at room temperature. **a** Schematic illustration of the thermodynamic calculation model. **b** In-plane misfit strain versus out-of-plane stress phase diagram of single-domain (111)-oriented [MDABCO]$(NH_4)I_3$ thin film. The inserts are schematics of the polarization direction for each phase.

coherency, the schematics is given in Fig. 2a. The stress and strain components in the global coordinate system satisfy the mixed mechanical boundary condition: $\sigma_4' = \sigma_5' = 0, \sigma_3' = \sigma$ and $\varepsilon_1' = \varepsilon_2' = u_m, \varepsilon_6' = 0$. The calculated stress and misfit strain intervals are 0.01 GPa and 0.001, respectively. Supplementary Fig. 2 shows the contour plots for the equilibrium polarization components P_x, P_y, and P_z in the pseudocubic system as a function of the misfit strain and external stress. It can be observed that the P_x, P_y, and P_z components have finite values at the low-stress region (see the R and M parts of the contour plot). In the high stress and high misfit strain regions, the cubic phase is stable where all polarization components vanish (the C-region in the phase diagram). In the O region (orthorhombic phase), the P_x and P_y components are in the same magnitudes while P_z equals zero.

Figure 2b shows the stable phases for (111)-oriented [MDABCO]$(NH_4)I_3$ thin films under different in-plane misfit strains and out-of-plane stresses at room temperature. There are four stable phases in total, depending on the misfit strain and applied stress. When the in-plane misfit strains are zero, the stable phase is orthorhombic O ($P_x^2 = P_y^2 \neq 0$, $P_z^2 = 0$) for $\sigma_{33} < -2.0$ GPa, monoclinic M ($P_x^2 = P_y^2 > P_z^2 \neq 0$) for $-2.0\ \text{GPa} \leq \sigma_{33} \leq 0.0$ GPa, and rhombohedral R ($P_x^2 = P_y^2 = P_z^2 \neq 0$) for $\sigma_{33} \geq 0.0$ GPa, respectively. In the region where both the in-plane misfit strain and the out-of-plane stress are highly negative, the cubic phase C ($P_x^2 = P_y^2 = P_z^2 = 0$) is stable. In this case, the mechanical condition applied to the material is similar to a hydrostatic pressure, which could favor the paraelectric cubic phase. Notably, no stable T-phase can be observed in the entire phase diagram. This can be understood since R-phase is the ground state for [MDABCO]$(NH_4)I_3$ and the film is (111)-oriented. T-phase has much higher energy as compared to the O phase according to the calculations from Wang et al.[16], which is difficult to stabilize via strain engineering in (111)-oriented [MDABCO]$(NH_4)I_3$ thin films.

Elastocaloric effect

With the knowledge of the dependence of stress and epitaxial strain on the polarization, now we proceed to calculate the eC

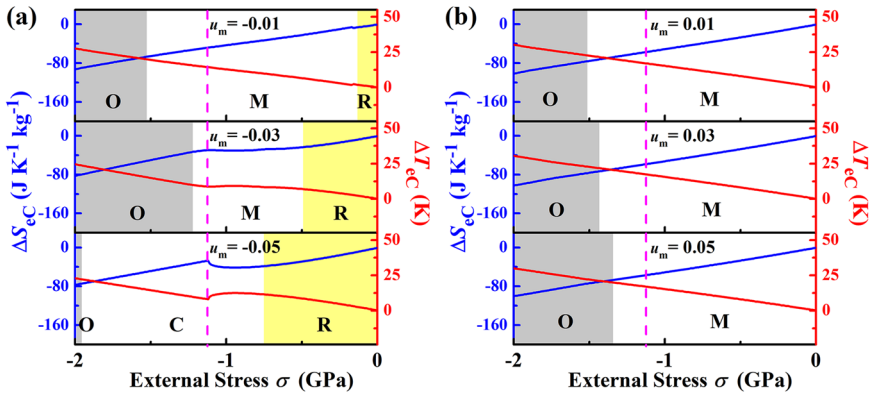

Fig. 3 The eC performance of the [MDABCO](NH4)I3 thin film as a function of external stress and substrate misfit strain. The eC entropy change ΔS_{eC} and the eC temperature change ΔT_{eC} under external stress for $[MDABCO](NH_4)I_3$ thin film with **a** compressive misfit strains and **b** tensile misfit strains. The gray, white, and yellow regions mark different phases. The blue line shows the entropy change, while the red line indicates the temperature change. The pink dash line marks the maximum nonuniform directional stress −1.28 GPa above which the system undergoes plastic deformation.

Table 1. Comparison of elastocaloric properties for different materials from previous literature and $[MDABCO](NH_4)I_3$ thin films in this study.

Material	T (K)	$\lvert\Delta\sigma\rvert$ (GPa)	$\lvert\Delta T_{eC}\rvert$ (K)	$\lvert\Delta T_{eC}/\Delta\sigma\rvert$ (K GPa^{-1})	$\lvert\Delta S_{eC}\rvert$ (J K^{-1} kg^{-1})	RC (J kg^{-1})	COP	Ref.	Method[a]
TiNiFe	293	/	4.8	/	/	/	4.90	[32]	Thermo
PVDF	300	0.015	2	133	11	22	/	[38,39]	Ex.
$PbTiO_3$	700	1	20	20	/	/	/	[18]	DFT
$PbZrO_3$	950	2	25	12.5	/	/	/	[46]	DFT
PMN-32PT	323	0.028	0.36	12.9	/	/	/	[20]	Ex.
$PbZr_{0.2}Ti_{0.8}O_3$	298	2	11	5.5	/	/	/	[47]	PF
$BaTiO_3$	300	6.5	4.6	0.7	8.7	40	0.003	[1,21]	Thermo
$Ba_{0.5}Sr_{0.5}TiO_3$	260	1	9	9	/	/	/	[17]	DFT
BCZT	340	0.25	1.5	6	/	/	/	[48]	Ex.
$Bi_4Ti_3O_{12}$	900	2	8.8	4.4	/	/	/	[49]	DFT
$[MDABCO](NH_4)I_3$	298	1.28	22.9	17.9	76.85	1760	1.11	this work	Thermo

[a]Ex., DFT, PF, and Thermo stands for experimental, first principle calculations, phase-field simulations, and thermodynamic calculations, respectively.

properties. Figure 3 shows the eC entropy change ΔS_{eC} and temperature change ΔT_{eC} versus the out-of-plane compressive stress for various $[MDABCO](NH_4)I_3$ thin films under different misfit strains (u_m). To calculate the variations of the ΔS_{eC} and ΔT_{eC} with the phase change, compressive stress is applied on top of the thin film. With the increase of the applied stress, phase transitions from rhombohedral (R) to monoclinic (M) or cubic (C) and finally to orthorhombic (O) occur. According to the previous report[37], $[MDABCO](NH_4)I_3$ undergoes a plastic deformation when the unidirectional compressive stress is above 1.28 GPa, which is set as the upper limit of the applied stress for the calculations in this study. Note that to sustain 1.28 GPa for the whole thin film device, one has to find either suitable oxide wafers or ductile metals as substrate, or even freestanding film without substrate. Assuming a constant heat capacity of 1000 J K^{-1} kg^{-1} for $[MDABCO](NH_4)I_3$ at room temperature[16], the maximum adiabatic temperature change ΔT_{eC} ~18.7 K occurs with $u_m = -0.01$. In most cases, with the highest applied stress, the adiabatic temperature change can reach 10–20 K as shown in Fig. 3a, while the maximum adiabatic temperature change is 22.9 K with a tensile misfit strain of 0.01 as shown in Table 1. Interestingly, at the large compression side (e.g., $u_m = -0.05$ and −0.03), ΔS_{eC} (ΔT_{eC}) shows a nonlinear relationship with the external stress while for all the other cases mainly linear dependency is obeserved.

Table 1 and Supplementary Fig. 4 summarize the eC properties for $[MDABCO](NH_4)I_3$ and other ferroelectrics that has been reported recently. For the polyvinylidene fluoride (PVDF) based ferroelectric polymers, the polar to the nonpolar phase transition is very sensitive to external mechanical stresses. High eC effects have been reported and adiabatic temperature changes of ~2 K were measured directly in PVDF polymers near room temperature under uniaxial stresses of ~10 MPa[38,39]. Meanwhile, some typical ferroelectric perovskite thin films also present finite eC effects at room temperature. For instance, $BaTiO_3$ thin films show a ΔT_{ec}~ 5 K under huge uniaxial stress of 6.5 GPa[1,21]. On the other hand, $PbTiO_3$ thin film exhibit a maximum adiabatic temperature change of ~20 K[18], which has been ascribed to the mixed ferroelastic and ferroelectric behaviors. However, such a giant eC effect can only occur at ~700 K, which is too high for practical applications. In comparison, $[MDABCO](NH_4)I_3$ displays considerably high eC strength, which is much higher than traditional lead-free ferroelectric perovskites, as shown in the light gray area of Supplementary Fig. 4. Polymer-based ferroelectrics have been found to exhibit higher temperature change ΔT_{ec}, but they have a very low refrigerant capacity ($RC = |\Delta T^* \Delta S|$). The calculated RC performance of $[MDABCO](NH_4)I_3$ thin film is 1760 J kg^{-1}, much superior to other ferroelectrics as reported in the previous literature. The coefficient of performance (COP) is another commonly used metric to describe the efficiency of the cooling

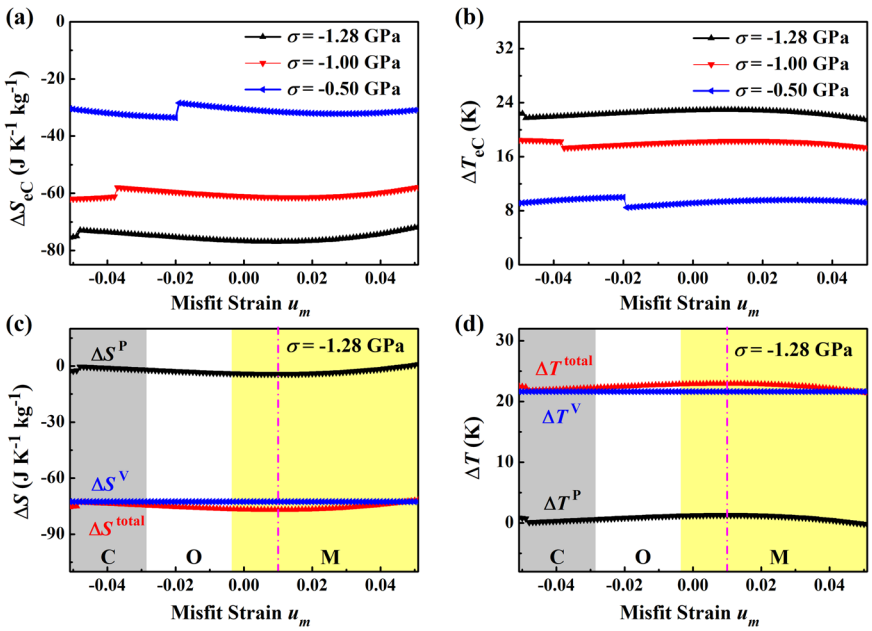

Fig. 4 Contributions of the eC performance of the $[MDABCO](NH_4)I_3$ thin film. a The eC entropy change ΔS_{eC} and **b** the eC temperature change ΔT_{eC} for $[MDABCO](NH_4)I_3$ thin film versus with misfit strain (u_m) under different external stresses. The contributions of polarization change and volume change under a compressive stress of 1.28 GPa for **c** the eC entropy change and **d** the eC temperature change ΔT_{eC}. The gray, white, and yellow regions mark different phases. The pink dash lines mark the maximum eC ΔS_{eC} and ΔT_{eC} at a stress of −1.28 GPa.

cycle, which is defined as the ratio of the cooling power (Q) to the input work (W) required to perform a thermodynamic cycle. As listed in Table 1, the calculated COP of $[MDABCO](NH_4)I_3$ thin film is about 1.11, which is much higher as compared to the other ferroelectrics such as $BaTiO_3$ and comparable to the widely used eC materials such as TiNiFe shape memory alloys[32].

Now we further turn to discuss the detailed underlying mechanisms for the superior eC performance of $[MDABCO](NH_4)I_3$. Figure 4 demonstrates the eC entropy change ΔS_{eC}, and the eC temperature change ΔT_{eC} for $[MDABCO](NH_4)I_3$ thin films under different in-plane misfit strains (u_m) and out-of-plane stresses. With the increasing of the out-of-plane stress, both the magnitudes of ΔS_{eC} and ΔT_{eC} increase. Figure 4c, d show the contributions of volume change and polarization change to ΔS_{eC} and ΔT_{eC}, respectively. We choose a compressive stress of −1.28 GPa as an example, two contributions to ΔS_{eC} can be identified as follows. The ordering of the dipoles by the application of external stress under isothermal conditions leads to a reduction or increase in the dipole configurational entropy (ΔS^P), which is associated with the phase transitions. The other contribution is the volume change induced entropy change (ΔS^V) given by $\frac{\beta_i}{\rho}(\sigma_1+\sigma_2+\sigma_3)$, where the thermal expansion coefficient β_i and the mass density ρ, have both been evaluated in the previous paper[16]. For $[MDABCO](NH_4)I_3$ film, these two parts compete with each other when compressive stress is applied but the ΔS^V dominates the total entropy due to its characteristic of low Young's modulus, which is only one percent of the Young's modulus for typical ferroelectric oxides. The low Young's modulus prompts the high thermal expansion coefficient and thus results in the big entropy reduction when applying the compressive stress (see Fig. 4a, c).

Calculations of elastocaloric effect for inorganic oxide ferroelectrics

Moreover, the impact of physical properties in materials on the eC strength is investigated, by calculating some common (111)-oriented ferroelectric oxide films using the same method. Material parameters are taken from existing publications for $BaTiO_3$ (BTO)[40], $PbTiO_3$ (PTO)[41], $PbZr_{0.52}Ti_{0.48}O_3$ (PZT-0.52)[42], $PbZr_{0.8}Ti_{0.2}O_3$ (PZT-0.8)[42], $K_{0.5}Na_{0.5}NbO_3$ (KNN)[43,44], and $KNbO_3$ (KNO)[44] thin films, respectively. Figure 5a, b show the comparison of isothermal entropy change ΔS_{eC} and adiabatic temperature change ΔT_{eC} between $[MDABCO](NH_4)I_3$ and other typical ferroelectric materials. The predicted eC strengths, isothermal $\Delta S_{eC}/\Delta\sigma$ and adiabatic $\Delta T_{eC}/\Delta\sigma$, for $[MDABCO](NH_4)I_3$ are $-60.0\ J\ K^{-1}\ kg^{-1}\ GPa^{-1}$ and $17.9\ K\ GPa^{-1}$, respectively, more than one order of magnitude higher than the largest value for oxide ferroelectric films. For example, the PTO film has the highest $\Delta T_{eC} = -24.70$ K, but measured under a considerably high stress $\Delta\sigma$ of 4.55 GPa. The calculated eC strength for PTO agrees well with the previous study by first principle calculation, in which the eC temperature change ΔT_{eC} is ~7 K under a stress $\Delta\sigma$ of 1.4 GPa[18]. Moreover, the calculated eC strength $|\Delta T_{eC}/\Delta\sigma|$ of $0.76\ K\ GPa^{-1}$ for $BaTiO_3$ film is consistent with Liu et al.[1]. Other ferroelectric oxides such as $KNbO_3$ and $K_{0.5}Nb_{0.5}O_3$ thin films also show high ΔT_{eC} values under remarkably high compressive stress $\Delta\sigma$. In comparison, the $[MDABCO](NH_4)I_3$ thin film exhibits a high value of ΔS_{eC} ($-76.85\ J\ K^{-1}\ kg^{-1}$) and ΔT_{eC} (22.9 K) under a lower $\Delta\sigma$ of 1.28 GPa. The outstanding eC strength of $[MDABCO](NH_4)I_3$ film can be understood by separating the contributions from two parts. For the polarization change induced eC temperature change ($|\Delta T^P/\Delta\sigma|$), the value of $[MDABCO](NH_4)I_3$ is in the same order of magnitude as the value of the oxide perovskites. But for the volume change induced eC temperature change ($|\Delta T^V/\Delta\sigma|$), due to the high compressibility of $[MDABCO](NH_4)I_3$, it is one order of magnitude higher than the highest value of the other ferroelectric films. The specific value for the eC properties of the above ferroelectric films could be found in Supplementary Table 4 and Supplementary Figs. 5, 6.

DISCUSSION

Following the previous results, we further identify several intrinsic physical properties, namely the elastic compliance s_{ij}, thermal expansion coefficient β_i on the eC effects of the metal-free

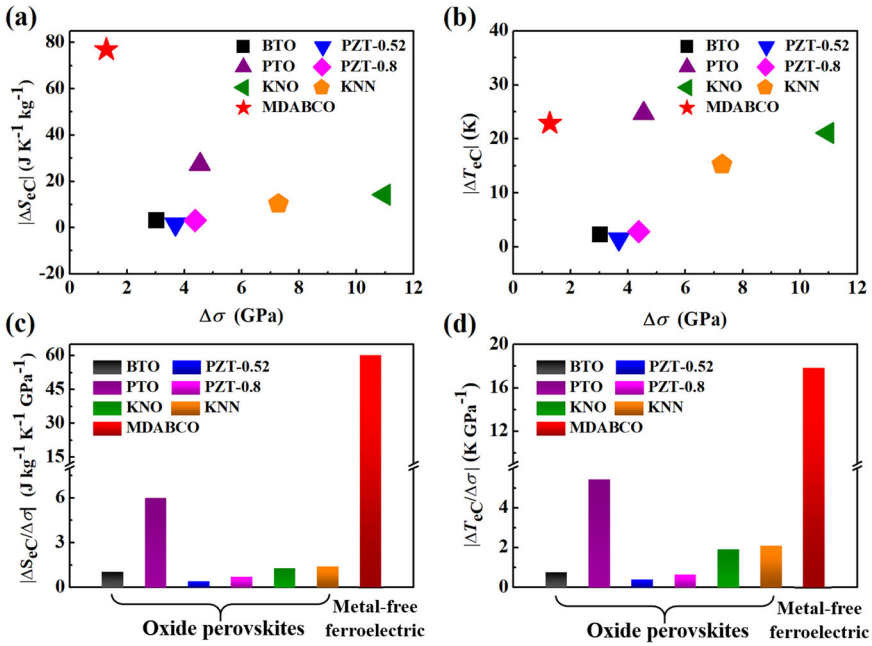

Fig. 5 Comparisons of the eC performance between [MDABCO](NH4)I3 and other ferroelectric thin films from thermodynamic calculations. a The eC entropy change $|\Delta S_{eC}|$, **b** the eC temperature change $|\Delta T_{eC}|$, **c** the eC strength $|\Delta S_{eC}/\Delta\sigma|$, and **d** the eC strength $|\Delta T_{eC}/\Delta\sigma|$.

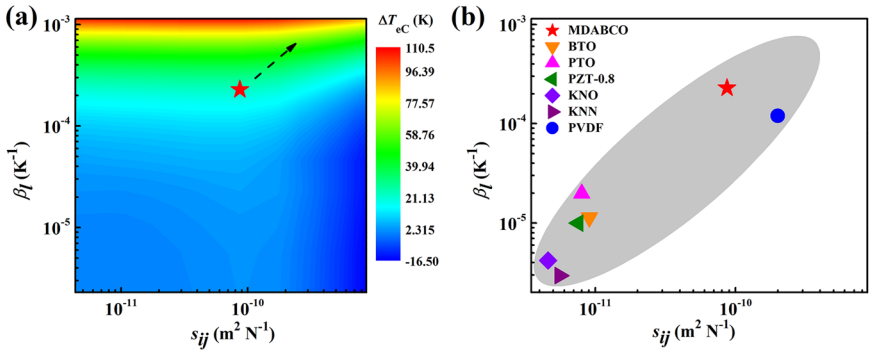

Fig. 6 Design space for high eC materials with respect to the linear thermal expansion and elastic compliance. a Two-dimensional plot of the evaluated eC temperature change ΔT_{eC} for $[MDABCO](NH_4)I_3$ based metal-free ferroelectrics as a function of β_l and s_{ij}. The red star represents the $[MDABCO](NH_4)I_3$ and the dashed arrow points out the direction for the design of organic ferroelectrics with high eC properties. **b** The thermal expansion coefficient β_l and elastic compliance s_{ij} for different ferroelectrics. The compressive stress and the misfit strain are fixed at 1.28 GPa and 0.01, respectively.

ferroelectrics, hoping to find design principles for high eC materials. The calculated eC temperature changes ΔT_{eC} is plotted in Fig. 6 and Supplementary Fig. 6, by varying the values of the above-mentioned material properties. Figure 6a shows a two-dimensional plot of the temperature change ΔT_{eC} as a function of both elastic compliance and thermal expansion. It is indicated that generally, eC decreases with increasing of elastic compliance, while increases with increasing thermal expansion coefficient. A relatively stronger dependency on β_l can be observed. For instance, ΔT_{eC} shows a dramatic increase to ~100 K with increasing of the β_l to five times of $[MDABCO](NH_4)I_3$ with fixing of the elastic compliance (Supplementary Fig. 6).

Note that the elastic compliance and thermal expansion coefficient are not independent physical parameters for a certain material. We map out the elastic compliance and thermal expansion coefficients of several oxide ferroelectrics, PVDF, and $[MDABCO](NH_4)I_3$ in Fig. 6b. The thermal expansion coefficient increases along with the increases of elastic compliance for almost all ferroelectric materials. Compared to oxide ferroelectric films, metal-free ferroelectric $[MDABCO](NH_4)I_3$ film has higher elastic compliance that will surpress the eC effect, but the higher thermal expansion coefficient has a higher influence on the eC performance, resulting in one order of magnitude higher in eC strength. Furthermore, modifying the cation $[MDABCO]^{2+}$ and anion I^- in the $[MDABCO](NH_4)I_3$ crystal could change the physical properties including the thermal expansion coefficient and elastic compliance[25,45]. Thus, theoretically, by rational design of the composition of the $[MDABCO](NH_4)I_3$ film, the eC performance in ferroelectrics can be further improved by enhancing the thermal expansion coefficient of the organic ferroelectrics.

In summary, we have developed a thermodynamic description for (111)-oriented organic ferroelectric $[MDABCO](NH_4)I_3$ thin film and investigated its phase transition behavior and eC properties under different misfit strains and applied external stresses. We found that there are two contributions to the eC strength, namely the polarization changes induced entropy change (ΔS^P) and the volume change induced entropy change (ΔS^V), which competes with each other under compressive stress. For organic ferroelectric materials which are relatively soft, the entropy change ΔS^V dominates, which is an order of magnitude higher than traditional ferroelectric oxides. It

is demonstrated that an eC entropy change of $-65.4\ J\ kg^{-1}\ K^{-1}$ and an adiabatic eC temperature change of 22.9 K are achieved for $[MDABCO](NH_4)I_3$ under a compressive stress of 1.28 GPa at a misfit strain of 0.01. This can be attributed to the low Young's modulus of $[MDABCO](NH_4)I_3$, which is only one percent of Young's modulus of conventional oxides. By analyzing the relationship of eC with thermal expansion coefficient and elastic compliance, we further discovered that the thermal expansion coefficient has a dominant role in determining the eC. Based on our theoretical analysis, we predict that it is possible to further improve the eC properties by enhancing the thermal expansion coefficient through chemical modification of the $[MDABCO](NH_4)I_3$. We envision this work will attract broad interest from the community of solid eC materials.

METHODS

Thermodynamic calculations of ferroelectric thin films

Based on the Landau-Devonshire theory, there are mainly four contributions in the total thermodynamic free energy density:

(1) Polarization energy $G_{polarization} = a_i P_i + a_{ij} P_i P_j + a_{ijk} P_i P_j P_k + a_{ijkl} P_i P_j P_k P_l + a_{ijklm} P_i P_j P_k P_l P_m + a_{ijklmn} P_i P_j P_k P_l P_m P_n$,

(2) thermal energy $G_{thermal} = -c_p T \ln \frac{T}{T_0} + c_p (T - T_0)$,

(3) mechanical energy $G_{Mechanic} = \frac{1}{2} C_{ijkl} (\varepsilon_{ij} - \varepsilon_{ij}^{\circ})(\varepsilon_{kl} - \varepsilon_{kl}^{\circ})$

And (4) electric energy $G_{electric} = -E_i P_i - \frac{1}{2} K_{ij} \varepsilon_0 E_i E_j$.

Where a_i, a_{ij}, a_{ijk}, a_{ijkl}, a_{ijklm}, and a_{ijklmn} are the Landau coefficients, and c_p, C_{ijkl}, K_{ij}, ε_0, and E_i represent the heat capacity, elastic modulus tensor, background dielectric constants, permittivity of vacuum, and electric fields. P_i, T, and T_0 are the polarization components, temperature, and romm temperature, respectively. The eigen strain is defined as $\varepsilon_{ij}^{\circ} = Q_{ijkl} P_k P_l + R_{ijklm} P_k P_l P_m + \beta_l (T - T_0)$

Here Q_{ijkl} and R_{ijklm} are the electromechanical strictive tensors. β_l is the linear thermal expansion coefficient. Consider a paraelectric-ferroelectric phase transition from high symmetry cubic phase (with space group P432) to rhombohedral phase (space group R3), expanding the polynomials to eighth order, neglecting all the symmetry forbidden terms, one can rewrite:

$$\begin{aligned}\Delta G =\ & a_1(P_1^2+P_2^2+P_3^2) + a_{11}(P_1^4+P_2^4+P_3^4)\\ & + a_{12}(P_1^2P_2^2+P_1^2P_3^2+P_2^2P_3^2) + a_{111}(P_1^6+P_2^6+P_3^6)\\ & + a_{112}\left[P_1^2(P_2^4+P_3^4)+P_2^2(P_1^4+P_3^4)+P_3^2(P_1^4+P_2^4)\right]\\ & + a_{123}P_1^2P_2^2P_3^2 + a_{1111}(P_1^8+P_2^8+P_3^8) + a_{1122}(P_1^4P_2^4+P_2^4P_3^4+P_1^4P_3^4)\\ & + a_{1112}\left[P_1^6(P_2^2+P_3^2)+P_2^6(P_1^2+P_3^2)+P_3^6(P_1^2+P_2^2)\right]\\ & + a_{1123}(P_1^4P_2^2P_3^2+P_2^4P_1^2P_3^2+P_3^4P_1^2P_2^2) - \tfrac{1}{2}s_{11}(\sigma_1^2+\sigma_2^2+\sigma_3^2)\\ & - s_{12}(\sigma_1\sigma_2+\sigma_1\sigma_3+\sigma_2\sigma_3) - \tfrac{1}{2}s_{44}(\sigma_4^2+\sigma_5^2+\sigma_6^2)\\ & - Q_{11}(\sigma_1P_1^2+\sigma_2P_2^2+\sigma_3P_3^2)\\ & - Q_{12}\left[\sigma_1(P_2^2+P_3^2)+\sigma_3(P_1^2+P_2^2)+\sigma_2(P_1^2+P_3^2)\right]\\ & - Q_{44}(P_2P_3\sigma_4+P_1P_3\sigma_5+P_1P_2\sigma_6)\\ & - \beta_l(\sigma_1+\sigma_2+\sigma_3)(T-T_0)\\ & - \lambda_{eff}\left[\sigma_6(P_1^2-P_2^2)P_3+\sigma_5(P_3^2-P_1^2)P_2+\sigma_4(P_2^2-P_3^2)P_1\right]\\ & - E_1P_1 - E_2P_2 - E_3P_3 - \tfrac{1}{2}\varepsilon_0(K_{11}E_1^2+K_{22}E_2^2+K_{33}E_3^2\\ & + K_{12}E_1E_2+K_{13}E_1E_3+K_{23}E_2E_3).\end{aligned} \quad (1)$$

Where the *α-terms* are the simplified Landau coefficients, s_{11}, s_{12}, and s_{44} are the elastic compliance, $\sigma_i (i = 1, 6)$ are the stresses, λ_{eff} is the high-order electrostrictive term. E_i are the applied electric fields, K_{ij} are the relative dielectric constants.

We then transfer the polarization and stresses from the local coordinate system $\boldsymbol{x}$ to the global coordinate system $\mathbf{x}'$ by using the transformation matrix $\boldsymbol{t_{ij}}$:

$$t_{ij} = \begin{pmatrix} \frac{1}{\sqrt{2}} & -\frac{1}{\sqrt{2}} & 0 \\ \frac{1}{\sqrt{6}} & \frac{1}{\sqrt{6}} & -\frac{2}{\sqrt{6}} \\ \frac{1}{\sqrt{3}} & \frac{1}{\sqrt{3}} & \frac{1}{\sqrt{3}} \end{pmatrix}. \quad (2)$$

For the epitaxial thin film with the in-plane misfit strains of ε_1' and ε_2' (the strain in global coordinate), the free energy $\Delta G'$ can be derived using the Legendre transformation

$$\Delta G' = \Delta G + \varepsilon_1'\sigma_1' + \varepsilon_2'\sigma_2' = \Delta G + u_m(\sigma_1' + \sigma_2'). \quad (3)$$

In Eq. 3, the misfit strains ε_1' and ε_2' are the same for a cubic substrate.

For the epitaxial film under typical in-plane biaxial misfit strains and out-plane stress in a global coordinate system, it is subjected to a mixed mechanical boundary condition with

$$\partial G'/\partial \sigma_i' = -\varepsilon_i', \varepsilon_1' = \varepsilon_2' = u_m,\ \varepsilon_6' = 0,\ \sigma_3' = \sigma_{app},\ \sigma_4' = \sigma_5' = 0. \quad (4)$$

in which the ε_1' and ε_2' are the in-plane strains, the ε_6' is the shear strain, the σ_3' is the out-plane stress along [111] direction, and the σ_4' and σ_5' are the in-plane stresses.

Assuming the film is pre-polarized in the electric field, the polarization ($_{Pi}$) under given misfit strains and out-plane applied stress at room temperature can be obtained by minimizing the thermodynamic free energy density $\Delta G'$ with respect to polarization $_{Pi}$.

Establishment of phase diagrams

The phase evolutions under applied stress at different misfit strains for $[MDABCO](NH_4)I_3$ thin films are thoroughly investigated and exhibited in Fig. 2 after we obtained the magnitude of the polarization components. Here we also employ the thermodynamic method to explore the phase evolutions for common ferroelectrics including $BaTiO_3$, $PbTiO_3$, $PbZr_{0.52}Ti_{0.48}O_3$, $PbZr_{0.8}Ti_{0.2}O_3$, $K_{0.5}Na_{0.5}NbO_3$, and $KNbO_3$. The stress versus misfit strain phase diagrams for these ferroelectric films at room temperature are displayed in Supplementary Fig. 3.

Calculation of elastocaloric effect

The total isothermal eC entropy change per mass under an application of stress σ_{app} at room temperature can be calculated by $\Delta S_{eC} = -\frac{1}{\rho}\left(\frac{\partial \Delta G'}{\partial T}\right)_{\sigma_{ij}}$ and it is derived from two parts:

(1) the polarization configuration change

$$\begin{aligned}\Delta S^{P} &= \Delta S_{dipole}(298\ K, \sigma = \sigma_{app}) - \Delta S_{dipole}(298\ K, \sigma = 0)\\ &= -\frac{1}{\rho}\left(\frac{da_1(T)}{dT}\left(P_i^2|_{\sigma=\sigma_{app}} - P_i^2|_{\sigma=0}\right) + \frac{da_{111}(T)}{dT}\left(P_i^6|_{\sigma=\sigma_{app}} - P_i^6|_{\sigma=0}\right)\right),\end{aligned} \quad (5)$$

and (2) the stress-induced volume change

$$\Delta S^{V} = \Delta S_{lattice}(298\ K, \sigma = \sigma_{app}) - \Delta S_{lattice}(298\ K, \sigma = 0) = \frac{\beta_l}{\rho}(\sigma_1 + \sigma_2 + \sigma_3). \quad (6)$$

Under the reversible adiabatic condition, the total entropy is conserved upon a stress change, thus we can obtain

$$\begin{aligned}\Delta T_{eC} = & \frac{T}{c_p\rho}\left(\frac{da_1(T)}{dT}\left(P_i^2|_{\sigma=\sigma_{app}} - P_i^2|_{\sigma=0}\right) + \frac{da_{111}(T)}{dT}\left(P_i^6|_{\sigma=\sigma_{app}} - P_i^6|_{\sigma=0}\right)\right)\\ & - \frac{T\beta_l}{c_p\rho}(\sigma_1 + \sigma_2 + \sigma_3).\end{aligned} \quad (7)$$

All the physical parameters and all coefficients can be found in Supplementary Tables 1 and 2 in the Supporting Information.

The COP can be evaluated by the following equation:

$$COP = \frac{Q}{W} \quad (8)$$

in which Q represents the absorbed heat and W is the specific mechanical work in the eC cooling cycle. The absorbed heat Q is derived from $\int TdS$, in which the T and S are the temperature and entropy, respectively. The specific mechanical work W is calculated by $\frac{1}{\rho}\int \sigma d\varepsilon$, in which the ρ, σ, and ε are the mass density, stress, and strain, respectively.

DATA AVAILABILITY

The raw data for the thermodynamic calculations in this paper and its supplemental information files are available from the corresponding author (hongzijian100@zju.edu.cn) upon reasonable request.

CODE AVAILABILITY

The code for the thermodynamic calculations in this paper and its supplemental information files are available from the corresponding author (hongzijian100@zju.edu.cn) upon reasonable request.

Received: 27 February 2021; Accepted: 26 July 2021;
Published online: 16 August 2021

REFERENCES

1. Liu, Y., Infante, I. C., Lou, X., Bellaiche, L., Scott, J. F. & Dkhil, B. Giant room-temperature elastocaloric effect in ferroelectric ultrathin films. *Adv. Mater.* **26**, 6132–6137 (2014).
2. Bruederlin, F., Bumke, L., Chluba, C., Ossmer, H., Quandt, E. & Kohl, M. Elastocaloric cooling on the miniature scale: a review on materials and device engineering. *Energy Technol.* **6**, 1588–1604 (2018).
3. Choi, S., Han, U., Cho, H. & Lee, H. Review: recent advances in household refrigerator cycle technologies. *Appl. Therm. Eng.* **132**, 560–574 (2018).
4. Franco, V., Blázquez, J. S., Ipus, J. J., Law, J. Y., Moreno-Ramírez, L. M. & Conde, A. Magnetocaloric effect: from materials research to refrigeration devices. *Prog. Mater. Sci.* **93**, 112–232 (2018).
5. Brück, E. Developments in magnetocaloric refrigeration. *J. Phys. D Appl. Phys.* **38**, R381–R391 (2005).
6. Scott, J. F. Electrocaloric materials. *Annu. Rev. Mater. Res.* **41**, 229–240 (2011).
7. Fähler, S. et al. Caloric effects in ferroic materials: new concepts for cooling. *Adv. Eng. Mater.* **14**, 10–19 (2012).
8. Liu, Y., Scott, J. F. & Dkhil, B. Direct and indirect measurements on electrocaloric effect: recent developments and perspectives. *Appl. Phys. Rev.* **3**, 031102 (2016).
9. Mangeri, J., Pitike, K. C., Alpay, S. P. & Nakhmanson, S. Amplitudon and phason modes of electrocaloric energy interconversion. *Npj Comput. Mater.* **2**, 16020 (2016).
10. Lu, B. F. & Liu, J. Mechanocaloric materials for solid-state cooling. *Sci. Bull.* **60**, 1638–1643 (2015).
11. Manosa, L. & Planes, A. Mechanocaloric effects in shape memory alloys. *Philos. Trans. R. Soc. A* **374**, 20150310 (2016).
12. Mischenko, A. S., Zhang, Q., Scott, J. F., Whatmore, R. W. & Mathur, N. D. Giant electrocaloric effect in thin-film $PbZr_{0.95}Ti_{0.05}O_3$. *Science* **311**, 1270 (2006).
13. Neese, B. et al. Large electrocaloric effect in ferroelectric polymers near room temperature. *Science* **321**, 821 (2008).
14. Ožbolt, M., Kitanovski, A., Tušek, J. & Poredoš, A. Electrocaloric refrigeration: thermodynamics, state of the art and future perspectives. *Int. J. Refrig.* **40**, 174–188 (2014).
15. Valant, M. Electrocaloric materials for future solid-state refrigeration technologies. *Prog. Mater. Sci.* **57**, 980–1009 (2012).
16. Wang, J. J., Fortino, D., Wang, B., Zhao, X. & Chen, L. Q. Extraordinarily large electrocaloric strength of metal-free perovskites. *Adv. Mater.* **32**, 1906224 (2020).
17. Lisenkov, S. & Ponomareva, I. Giant elastocaloric effect in ferroelectric $Ba_{0.5}Sr_{0.5}TiO_3$ alloys from first-principles. *Phys. Rev. B* **86**, 104103 (2012).
18. Lisenkov, S., Mani, B. K., Chang, C. M., Almand, J. & Ponomareva, I. Multicaloric effect in ferroelectric $PbTiO_3$ from first principles. *Phys. Rev. B* **87**, 224101 (2013).
19. Wang, F. et al. Giant room temperature elastocaloric effect of $PbTiO_3$ ferroelectric materials with 90° domain structure. *RSC Adv.* **6**, 70557–70562 (2016).
20. Chauhan, A., Patel, S. & Vaish, R. Multicaloric effect in $Pb(Mn_{1/3}Nb_{2/3})O_{3\text{-}32}PbTiO_3$ single crystals. *Acta Mater.* **89**, 384–395 (2015).
21. Liu, Y. et al. Prediction of giant elastocaloric strength and stress-mediated electrocaloric effect in $BaTiO_3$ single crystals. *Phys. Rev. B* **90**, 104107 (2014).
22. Lloveras, P. et al. Colossal barocaloric effects near room temperature in plastic crystals of neopentylglycol. *Nat. Commun.* **10**, 1803 (2019).
23. Li, B. et al. Colossal barocaloric effects in plastic crystals. *Nature* **567**, 506–510 (2019).
24. Wang, H. et al. Large piezoelectric response in a family of metal-free perovskite ferroelectric compounds from first-principles calculations. *Npj Comput. Mater.* **5**, 17 (2019).
25. Sun, S. et al. Factors influencing the mechanical properties of formamidinium lead halides and related hybrid perovskites. *ChemSusChem* **10**, 3740–3745 (2017).
26. Ye, H.-Y. et al. Metal-free three-dimensional perovskite ferroelectrics. *Science* **361**, 151 (2018).
27. Li, W. & Ji, L. J. Perovskite ferroelectrics go metal free. *Science* **361**, 132 (2018).
28. Kasel, T. W., Deng, Z. Y., Mroz, A. M., Hendon, C. H., Butler, K. T. & Canepa, P. Metal-free perovskites for nonlinear optical materials. *Chem. Sci.* **10**, 8187–8194 (2019).
29. Fu, D.-W. et al. Diisopropylammonium bromide is a high-temperature molecular ferroelectric crystal. *Science* **339**, 425 (2013).
30. Liao, W.-Q. et al. A molecular perovskite solid solution with piezoelectricity stronger than lead zirconate titanate. *Science* **363**, 1206 (2019).
31. Lou, F., Gu, T., Ji, J. Y., Feng, J. S., Xiang, H. J. & Stroppa, A. Tunable spin textures in polar antiferromagnetic hybrid organic–inorganic perovskites by electric and magnetic fields. *Npj Comput. Mater.* **6**, 114 (2020).
32. Ossmer, H., Wendler, F., Gueltig, M., Lambrecht, F., Miyazaki, S. & Kohl, M. Energy-efficient miniature-scale heat pumping based on shape memory alloys. *Smart Mater. Struct.* **25**, 085037 (2016).
33. Hong, S. B., An, Y. & Yu, W.-R. Characterization and modeling of elastocaloric effects of shape memory poly(cyclooctene). *Appl. Phys. Lett.* **114**, 013904 (2019).
34. Guyomar, D., Li, Y., Sebald, G., Cottinet, P.-J., Ducharne, B. & Capsal, J.-F. Elastocaloric modeling of natural rubber. *Appl. Therm. Eng.* **57**, 33–38 (2013).
35. Luo, D., Feng, Y. & Verma, P. Modeling and analysis of an integrated solid state elastocaloric heat pumping system. *Energy* **130**, 500–514 (2017).
36. Tušek, J., Engelbrecht, K., Mañosa, L., Vives, E. & Pryds, N. Understanding the thermodynamic properties of the elastocaloric effect through experimentation and modelling. *Shap. Mem. Superelasticity* **2**, 317–329 (2016).
37. Ehrenreich, M. G. et al. Mechanical properties of the ferroelectric metal-free perovskite $[MDABCO](NH_4)I_3$. *Chem. Commun.* **55**, 3911–3914 (2019).
38. Patel, S., Chauhan, A., Vaish, R. & Thomas, P. Elastocaloric and barocaloric effects in polyvinylidene di-fluoride-based polymers. *Appl. Phys. Lett.* **108**, 072903 (2016).
39. Yoshida, Y., Yuse, K., Guyomar, D., Capsal, J.-F. & Sebald, G. Elastocaloric effect in poly(vinylidene fluoride-trifluoroethylene-chlorotrifluoroethylene) terpolymer. *Appl. Phys. Lett.* **108**, 242904 (2016).
40. Wang, J. J., Wu, P. P., Ma, X. Q. & Chen, L. Q. Temperature-pressure phase diagram and ferroelectric properties of $BaTiO_3$ single crystal based on a modified Landau potential. *J. Appl. Phys.* **108**, 114105 (2010).
41. Li, Y. L., Hu, S. Y., Liu, Z. K. & Chen, L. Q. Effect of substrate constraint on the stability and evolution of ferroelectric domain structures in thin films. *Acta Mater.* **50**, 395 (2002).
42. Li, Y. L., Choudhury, S., Liu, Z. K. & Chen, L. Q. Effect of external mechanical constraints on the phase diagram of epitaxial $PbZr_{1-x}Ti_xO_3$ thin films—thermodynamic calculations and phase-field simulations. *Appl. Phys. Lett.* **83**, 1608–1610 (2003).
43. Zhou, M.-J., Wang, J.-J., Chen, L.-Q. & Nan, C.-W. Strain, temperature, and electric-field effects on the phase transition and piezoelectric responses of $K_{0.5}Na_{0.5}NbO_3$ thin films. *J. Appl. Phys.* **123**, 154106 (2018).
44. Pohlmann, H., Wang, J.-J., Wang, B. & Chen, L.-Q. A thermodynamic potential and the temperature-composition phase diagram for single-crystalline $K_{1-x}Na_xNbO_3$ ($0 \le x \le 0.5$). *Appl. Phys. Lett.* **110**, 102906 (2017).
45. Zhang, H.-Y., Tang, Y.-Y., Shi, P.-P. & Xiong, R.-G. Toward the targeted design of molecular ferroelectrics: modifying molecular symmetries and homochirality. *Acc. Chem. Res.* **52**, 1928–1938 (2019).
46. Lisenkov, S., Mani, B. K., Cuozzo, J. & Ponomareva, I. Highly tunable piezocaloric effect in antiferroelectric $PbZrO_3$. *Phys. Rev. B* **93**, 064108 (2016).
47. Wang, F., Li, B., Ou, Y., Liu, L. F., Tian, L. & Wang, W. Multicaloric effects in $PbZr_{0.2}Ti_{0.8}O_3$ thin films with 90° domain structure. *Europhys. Lett.* **118**, 17005 (2017).
48. Chauhan, A., Patel, S. & Vaish, R. Elastocaloric effect in ferroelectric ceramics. *Appl. Phys. Lett.* **106**, 172901 (2015).
49. Xu, B. L., Li, B., Wang, F., Wang, J. B., Zhong, X. L. & Wang, W. Negative/positive elastocaloric effect associated with vortex domain in the $Bi_4Ti_3O_{12}$ ferroelectric nanoparticle. *Europhys. Lett.* **115**, 47006 (2016).

ACKNOWLEDGEMENTS

This work was financially supported by the National Natural Science Foundation of China (Nos. 51572237 and 51802280), the Fundamental Research Funds for the Central Universities (Nos. 2020QNA4005, 2020FZZX002-01, 2020FZZX003-04, and 2021FZZX003-02-03), the NSFC-Zhejiang Joint Fund for the Integration of Industrialization and Informatization (U1909212), the National Key R&D Program of China (Nos. 2018YFC0114902). Z.H. would like to acknowledge a startup grant from Zhejiang University. J.-J.W. and L.-Q.C. gratefully acknowledge the partial support from the Donald W. Hamer Foundation for the Hamer Professorship at Penn State.

AUTHOR CONTRIBUTIONS

Y.H.H., J.-J.W. and Z.H. conceived the idea and designed the project. C.L. and J.-J.W. performed the calculations. B.W. supported the thermodynamic calculations. C.L., Y.H.H., J.J.W., H.T. and Z.H. analyzed the data. L.-Q.C., Z.H., and Y.J.W. supervised the project. All authors contributed to the discussions and analyses of the data and approved the final version.

COMPETING INTERESTS

The authors declare no competing interests.

ADDITIONAL INFORMATION

Supplementary information The online version contains supplementary material available at https://doi.org/10.1038/s41524-021-00599-1.

Correspondence and requests for materials should be addressed to Y.H.H., J.-J.W. or Z.H.